



**HAL**  
open science

## Effect of different fuels on combustion instabilities in an annular combustor

Preethi Rajendram Soundararajan, Guillaume Vignat, D. Durox, Antoine Renaud, Sébastien Candel

► **To cite this version:**

Preethi Rajendram Soundararajan, Guillaume Vignat, D. Durox, Antoine Renaud, Sébastien Candel. Effect of different fuels on combustion instabilities in an annular combustor. *Journal of Engineering for Gas Turbines and Power*, 2021, 143 (3), pp.031007. 10.1115/1.4049702 . hal-03674709

**HAL Id: hal-03674709**

**<https://hal.science/hal-03674709>**

Submitted on 12 Jul 2022

**HAL** is a multi-disciplinary open access archive for the deposit and dissemination of scientific research documents, whether they are published or not. The documents may come from teaching and research institutions in France or abroad, or from public or private research centers.

L'archive ouverte pluridisciplinaire **HAL**, est destinée au dépôt et à la diffusion de documents scientifiques de niveau recherche, publiés ou non, émanant des établissements d'enseignement et de recherche français ou étrangers, des laboratoires publics ou privés.

# Effect of different fuels on combustion instabilities in an annular combustor

Preethi Rajendram Soundararajan\*, Guillaume Vignat, Daniel Durox, Antoine Renaud, Sébastien Candel  
EM2C Laboratory, CentraleSupélec and CNRS, Université Paris-Saclay, 91192, Gif-sur-Yvette, France.  
Email: preethi.rajendram-soundararajan@centralesupelec.fr

*Combustion instability in annular combustors of jet engines is a recurring issue. In the present study, the characteristics of instabilities for different fuels are investigated by combining the instability maps obtained in a laboratory-scale annular combustor equipped with multiple swirling spray injectors (MICCA-Spray) and flame describing functions (FDFs) from a single sector configuration (SICCA-Spray). Two types of liquid fuels are injected as hollow cone sprays: heptane, which is fairly volatile, and dodecane, which is less volatile. Experiments are also conducted with gaseous propane, perfectly premixed with air, which serves as a reference. An instability map is systematically drawn by varying the global equivalence ratio and thermal power. The data indicate that the amplitude and frequency of instabilities depend, for the same operating point, on the fuel injection conditions (premixed or spray) and fuel type. Overall trends show that premixed propane is unstable in a broad operating domain. Injection of liquid fuels induce changes in flame time lag that modify the unstable regions. For heptane, the instability map is closer to the propane reference map, whereas dodecane exhibits wider stable regions. An attempt is made to understand these features by examining the FDF, which gives the ratio of relative fluctuations in heat release rate to the relative fluctuations in velocity. The FDFs measured in a single sector configuration give access to gain and phase information that can be used to determine unstable bands and calculate an instability index guiding the interpretation of the differences in instabilities of the three fuels.*

## INTRODUCTION

Combustion instabilities pose serious problems in many high-performance devices such as rocket engines, aircraft engines, and gas turbines. These instabilities have undesirable consequences, including intense noise and vibrations, excessive heat loads to the combustor walls, flashback, and blow-off [1,2], and in some cases, they may even lead to mechanical failure [3]. Many instabilities associated with combustion occur as a result of complex coupling between flow, combustion, and acoustics. Unsteady combustion generates acoustic

waves, and when this happens in a resonant environment it may induce flow perturbations. Through intermediary mechanisms, this further leads to heat release rate disturbances, which under certain conditions may grow, and the system becomes unstable. This situation is encountered in modern gas turbine engines operating in lean premixed regimes to reduce NO<sub>x</sub> emissions. In these devices, the flames are aerodynamically anchored by swirling injectors, producing compact flames with relatively high power densities in an environment with low damping that are receptive to resonant coupling, eventually leading to combustion instabilities [4,5]. These engines when operated with liquid fuels, use spray atomizers. The spray can be strongly influenced by the acoustic pressure oscillations in the chamber, even if the high atomizing pressure ensures a constant flow rate in many configurations [6–11].

Combustion instability is most often linked to a time delay between reactant injection and combustion. This delay is associated with convection, mixing, and chemical conversion, and under liquid injection, it is also linked to atomization, vaporization, and droplet inertia. The present investigation is focused on the role of changes in time lag linked with the injection of three different fuels in an annular combustor. In a reference case, propane premixed with air is injected. In two other cases, heptane and dodecane are atomized in the form of a spray of droplets. Thus, the time lag is modified, and this directly changes the instability characteristics.

At this point, it is worth reviewing the literature that considers delay effects (or equivalently phase effects) on the development of combustion instabilities. In a pioneering work on the so-called “singing flame”, Lord Rayleigh [12] provided a stability criterion indicating that acoustic pressure and unsteady heat release rate fluctuations have to be in phase for instabilities to grow. This may be translated in terms of a time delay between the acoustic pressure oscillations and heat release rate fluctuations, providing a necessary condition for the growth of thermo-acoustic instabilities. The importance of time lags was underlined in the early work on rocket engine instabilities, most notably by Crocco and his co-workers [13,14]. It was recognized that the time delay involved in the conversion of liquid fuels to gaseous state before burning, and the additional time lag associated with mix-

---

\*Address all correspondence to this author.

ing and reaction of propellants could be sensitive to the instantaneous conditions prevailing in the thrust chamber. The time lag was considered to be especially important in the case of liquid fuels as it results from complex processes such as the atomization of fuel droplets followed by vaporization and mixing. Many studies have used this time lag concept to derive methods that could be employed to suppress instabilities by suitably timing the liquid fuel injection or controlling other flow parameters. Such methods have been successfully demonstrated by Lee et al. [15] and Yu et al. [16].

Several investigations have been carried out to study the mechanism of instability caused by the time lag associated with liquid fuels. Zhu et al. [17] performed a numerical study on a fuel-spray aero-engine combustor to investigate the oscillating behavior of spray flames due to pressure fluctuations, and concluded that modulations of airflow rates affect the fuel droplet size distribution, thus modifying the fuel-air ratio, and thereby changing the time delay. Eckstein et al. [6] performed experiments on an air-blast atomizer in a rich-quench-lean combustor and showed that their atomizer was sensitive to fluctuations of air velocity in the injector, generating different droplet sizes, thus varying the combustion delay and oscillations. The effect of air and liquid fuel flow modulations on instabilities were examined by Gajan et al. [7] and Kim et al. [8] in non-reactive conditions. It was shown in [7] that the modulations of air influence the atomization process generating a droplet density wave with varying evaporation rates. Depending upon the convection velocity of this wave, a time lag appears between pressure and heat release rate. Apeloig et al. [18] performed studies on an actual multi-point spray injector of an aeronautical combustor and showed that the airflow fluctuations in the injector perturbed the atomization process, creating a varying time delay that could either amplify or dampen the instabilities. Pillai et al. [11] used numerical simulation to study a thermoacoustic instability in a backward-facing step flame. They used liquid kerosene injected as a liquid jet in cross-flow. The fuel flow rate and atomization processes, modulated by the acoustic pressure fluctuations, amplified the instability. The large-eddy simulation (LES) reported by Tachibana et al. [19] for a single sector aero-engine combustor operating at high pressure with liquid fuel (Jet-A) indicates that a short time delay is linked to the evaporation and fuel-air mixing processes. In an experimental investigation of a premixed prevaporized combustor fed with heptane, Bernier et al. [20] found that the evaporation delay happens simultaneously with droplet convection to the combustion region so that this delay need not be added to the other delays in the analysis of the causes of combustion instability. Vignat et al. [9] used an LES to study a self-sustained combustion oscillation in a single injector test rig, namely SICCA-Spray, and reached a similar conclusion. However, this might not apply to fuels that are less volatile than heptane.

The preceding studies indicate that it is worth examining instability characteristics that may be linked to the nature and physical state of the fuel with the objective of identifying the time lags' origins, comparing them with those of purely gaseous and premixed injection, and sorting out con-

sequences in terms of instability. Although time lag effects associated with liquid fuels are relatively well documented in the combustion instability literature, the number of studies that deal with liquid sprays in annular combustors is relatively small. The annular configuration has, however, considerable importance because it is commonly found in jet engines and most gas turbines. One of the current laboratory-scale annular combustors, MICCA-Spray at the EM2C laboratory, exhibits large amplitude azimuthal instabilities when it is fed with liquid fuel [1,2]. Another annular rig used by the team of Dawson & Worth at NTNU is only operated with premixed ethylene and air [21,22]. Investigations carried out on these combustors have revealed different modes of azimuthal instabilities such as standing, spinning (clockwise or counter-clockwise), and slanted [23]. In addition, there have been LES performed on industrial annular combustors with spray injection [24,25] and a number of more theoretical investigations [26,27] of instabilities in annular chambers. The MICCA-Spray test rig has also been used (Prieur et al. [28]) to examine ignition dynamics under premixed propane, heptane, and dodecane injection, and it was concluded that the light-round time delay is maximum for less volatile fuel, indicating that evaporation induces additional time lags. As an extension to the previous studies, the current work focuses on azimuthal instabilities in the MICCA-Spray annular chamber using three different fuels. Propane ( $C_3H_8$ ), fully premixed with air, is considered as the reference, as it features no mixing, atomization, or evaporation delays. Two liquid fuels are considered, heptane ( $C_7H_{16}$ ) that is fairly volatile ( $T_{boil} = 371\text{ K}$ ) and is closer to the reference case, and dodecane ( $C_{12}H_{26}$ ), a heavier fuel that is less volatile ( $T_{boil} = 489\text{ K}$ ) and hence has a longer vaporization time than heptane. Developing a complete understanding of the underlying mechanism of instabilities in an annular combustor is quite challenging, and hence it is worth examining the phenomenon on a simplified single injector system that resembles one sector of the annular combustor. A familiar way to understand the flame dynamics and its response to acoustic perturbations is by measuring the flame transfer function (FTF), that determines the variation of heat release rate with respect to incoming acoustic fluctuations. However, using linear concepts to describe flame dynamics (as embodied in the FTF) cannot explain many phenomena such as limit cycle oscillations or mode switching. To account for the flame nonlinearity, it is convenient to use the flame describing function (FDF) framework. This was exemplified by Dowling [29] in a theoretical investigation of instabilities of a ducted flame. The effectiveness of this framework was demonstrated by Noiray et al. [30], who showed that it allowed retrieving most of the nonlinear features observed experimentally like frequency shifting as the amplitude is growing, mode switching, triggering, and hysteresis. FDF is an extension of FTF, and it represents the flame response depending on the frequency and amplitude of the incoming velocity perturbations. The FDF framework has been successfully used in many further studies to model flame dynamics [31,32]. The FDF determined in a single sector configuration is used in the present study to interpret the complex combus-

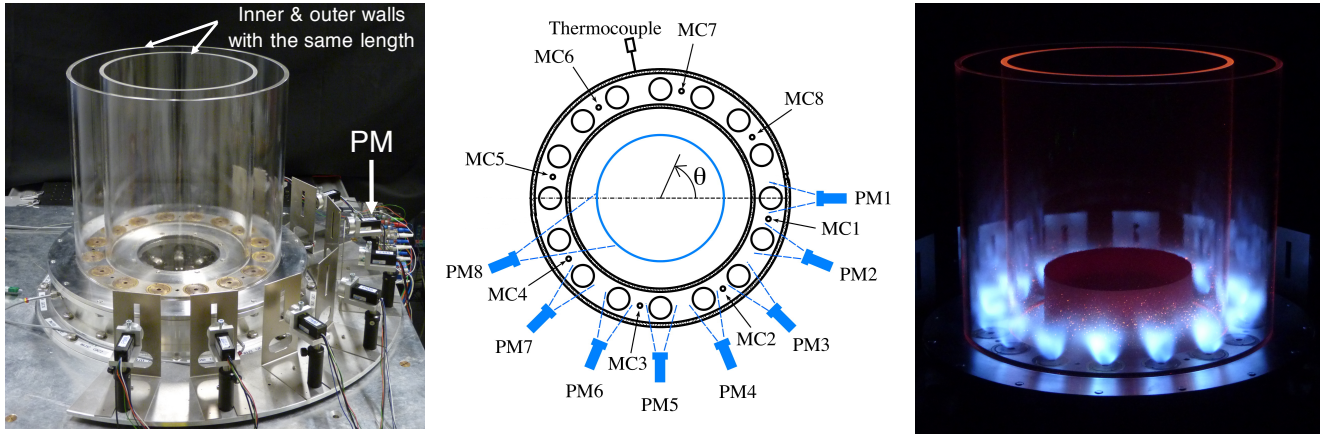


Fig. 1: From left to right: (1) Photograph of the MICCA-Spray test rig. (2) Schematic top view of the combustion chamber showing the locations of chamber microphones (MC $x$ ), the arrangement of photomultipliers (PM $x$ ), and the position of wall mounted thermocouple. The blue dashed lines show the field of view of each PM. A steel tube (marked as a blue circle) placed inside the inner chamber wall acts as a screen, preventing light transmission from opposite flames. The baseline for azimuthal angle is taken along the centreline of injector 1 and the positive direction of  $\theta$  is oriented in the counter-clockwise direction. Adapted from [2]. (3) Photograph of MICCA-Spray during operation.

tion dynamics observed in the MICCA-Spray configuration.

This article begins with a brief description of the experimental set-up for the annular configuration (MICCA-Spray) and the single injector system (SICCA-Spray) that is used for FDF measurements. Results of instability experiments in MICCA-Spray are systematically examined by varying the fuel types, equivalence ratio, and thermal power. The next section describes the FDFs obtained for the different fuels at three operating conditions in SICCA-Spray. The relation between MICCA-Spray instabilities and FDF results are then explored.

## EXPERIMENTAL SETUP

Two experimental setups are described successively: MICCA-Spray, which is a multiple injector annular combustor operating at atmospheric pressure, and SICCA-Spray, a single injector rig (one sector of MICCA-Spray) that is used to determine FDFs.

### MICCA-Spray

The MICCA-Spray test rig shown in Fig. 1 is a laboratory-scale annular combustor with multiple injection units. The system consists of an air plenum connected to the combustion chamber through sixteen spray-swirl injectors. The plenum is 80mm in height with an internal diameter of 280mm and an outer diameter of 420mm. The combustion chamber consists of two concentric, cylindrical, and vertical quartz walls of height 400mm, each with a thickness of 8mm. The inner quartz wall has an outer diameter of 300mm, while the outer quartz wall has an inner diameter of 400mm. The quartz walls provide optical access for the observation of the combustion region. Airflow is controlled through a Bronkhorst EL-FLOW mass flow controller with a relative accuracy better than 1%. Three fuels

are used in the present study: propane, heptane, and dodecane. Propane, being a gaseous fuel, is supplied through a Bronkhorst EL-FLOW mass flow controller and is premixed with air at ambient temperature before it enters the plenum. Liquid fuels, heptane and dodecane, are supplied through a Bronkhorst CORI-flow controller. The passage through the swirler channels results in a clockwise rotation of the flow with a measured swirl number of 0.71 (see [2] for swirler details). The flow enters into the combustion chamber through a conical section with an 8mm diameter outlet. For liquid fuel injection, a simplex atomizer forms a hollow cone spray of droplets. Ignition of MICCA-Spray is obtained by a spark plug introduced from the top of the chamber and removed before the measurements. This ensures rotational symmetry in the system's geometry. Twelve Bruel & Kjaer type 4938 microphones with type 2670 preamplifiers (with a relative accuracy of 1% and passband frequency between 15Hz and 20kHz) are used to record the acoustic pressure in the system. The measured signals are sampled at a frequency of 32,768 Hz. Four microphones are plugged on the plenum (designated as MP1 to MP4), while eight of them are mounted on the chamber (designated as MC1 to MC8 in Fig. 1). As the microphones cannot withstand the high temperatures prevailing in the chamber, they are flush mounted on waveguides formed by straight metallic tubes at a distance of 170mm from the chamber backplane resulting in a propagation time lag of 0.46ms [1]. The waveguide ports are located between every two injectors, and they are terminated by a 25m long tube in order to eliminate wave reflections. In addition to the pressure measurements, an array of eight photomultipliers (PMs) with OH\* filter (308nm) records the flame chemiluminescence (marked as PM1 to PM8 in Fig. 1). The suitability of using chemiluminescence as a qualitative indicator of heat release rate by flame dates back to experiments by Price et al. [33] for premixed flames. The case of

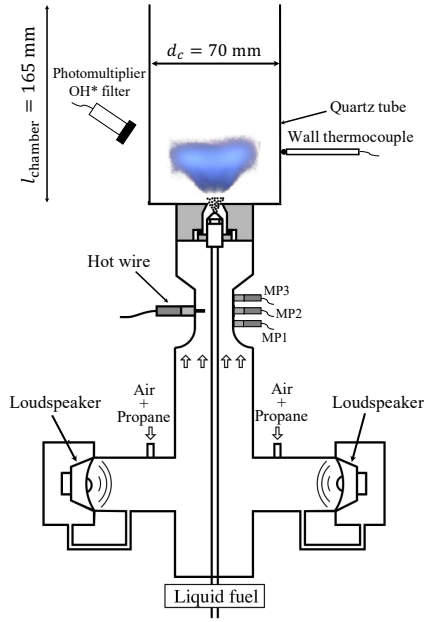


Fig. 2: Schematic of the experimental setup SICCA-Spray used for FDF measurements.

spray flames is considered by Mirat et al. [34]. Previous investigations carried out in MICCA-Spray [1] indicate that the instability depends on the wall temperature. Hence, a K-type thermocouple measures the temperature of the outer chamber wall to ensure that the system is thermally stabilized.

### SICCA-Spray

To interpret the self-sustained instabilities of MICCA-Spray, it is instructive to measure the FDF in a single sector device, SICCA-Spray. This experimental setup comprises a plenum connected to a combustion chamber through the same injection system used in MICCA-Spray. The schematic of the experimental setup is shown in Fig. 2. The system is acoustically excited by means of two driver units mounted in the plenum. Similar to MICCA-Spray, this system is used to study premixed (propane) as well as spray fuels (heptane and dodecane). When used in premixed conditions, propane is mixed with air at a distance of approximately 1 m from the plenum by a cyclone mixer. Mass flow rates are measured using a system similar to that of MICCA-Spray. The combustion chamber of SICCA-Spray has an internal diameter of 70 mm and is 165 mm long. Three microphones (designated as MP1 to MP3) measure the acoustic pressure upstream of the injector. A hot wire (Fig. 2) with Dantec miniCTA electronics records the velocity fluctuations. The acoustic velocity is also determined using the two-microphone technique [35,36] based on the pressure measurements in the plenum. This method, validated by comparing its results with hot wire velocity measurements, is especially desirable at higher amplitudes levels due to aliasing of hot wire measurements when the fluctuations exceed the mean velocity and the flow is reversed. Consider two microphones that are separated by

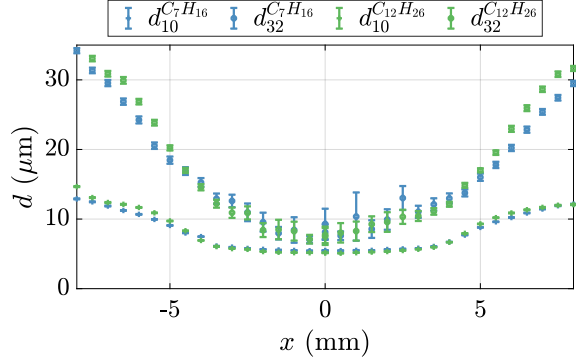


Fig. 3: Mean ( $d_{10}$ ) and Sauter mean diameter ( $d_{32}$ ) at different radial locations at a height of  $z=5$  mm above the backplane of SICCA-Spray.  $r=0$  represents the center of the injector and the error bars on the plot represent the statistical standard errors in the measurements.

a known distance  $\Delta x$ , and measuring 1D harmonic waves at a frequency  $f$ , the acoustic velocity is given by

$$u' = \frac{1}{i\rho_0\omega} \frac{p'_2 - p'_1}{\Delta x} \quad (1)$$

Here,  $p'_1$  and  $p'_2$  are the pressures measured by microphones MP1 and MP3 (refer Fig. 2) at the frequency  $f$  and angular frequency  $\omega = 2\pi f$ . The value of  $\Delta x$  is 39.4 mm and  $\rho_0 = 1.23 \text{ kg/m}^3$ . This method is precise only if the distance of separation is much smaller than the wavelength  $\lambda$  ( $\Delta x \ll \lambda$ ). The analytical signals for the microphone measurements are reconstructed using Hilbert transforms, and these complex signals are then used in Eq. (1). A photomultiplier equipped with an OH\* filter measures the flame chemiluminescence. In order to vary the amplitude of fluctuations for FDF measurements, the driver units are modulated at six different voltage levels  $V_0$  (300 mV to 1300 mV in steps of 200 mV) and a linear frequency sweep is performed from 200 Hz to 1100 Hz, at each level, for a time duration of 200 s. This procedure defines different levels of acoustic velocity fluctuations,  $u'/\bar{u}$  at the hot wire position. The measurements are recorded at a sampling frequency of 16,384 Hz.

Additionally, an intensified CCD camera (PI-MAX) with a CH\* filter (centered at 430 nm) and a  $1024 \times 1024$  spatial resolution is used to capture the time-averaged images of the flame. A Phase Doppler anemometer (PDA) from Dantec Dynamics is used for measuring the droplet size and velocity of the liquid spray. Measurements are performed at  $z=5$  mm above the chamber backplane at cold, unconfined condition. Figure 3 shows the distribution of mean ( $d_{10}$ ) and Sauter mean diameter ( $d_{32}$ ) at different locations above the backplane of the injector. It can be observed that there is not much variability in the droplet diameters ensuing from the spray between the two fuels.

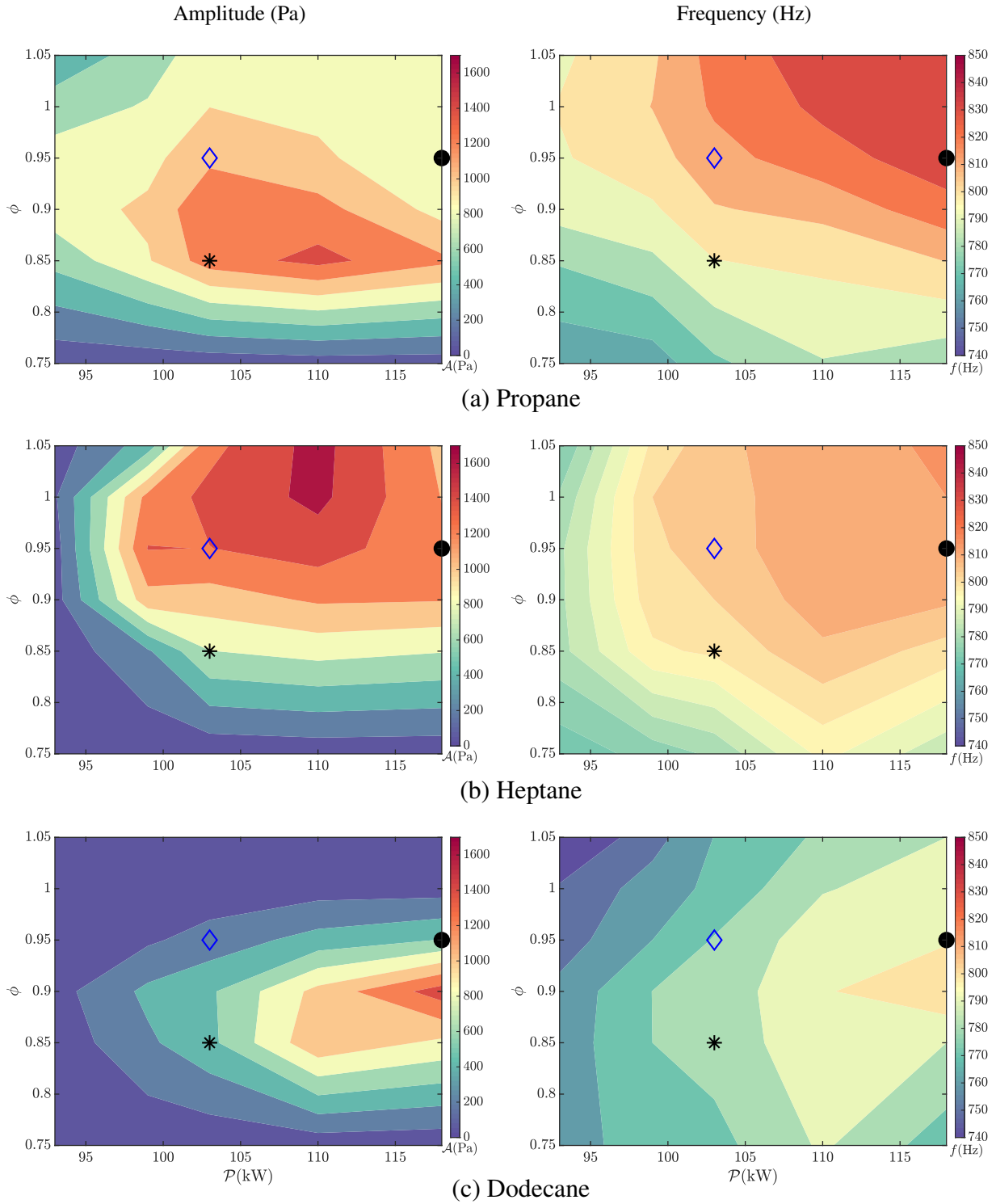
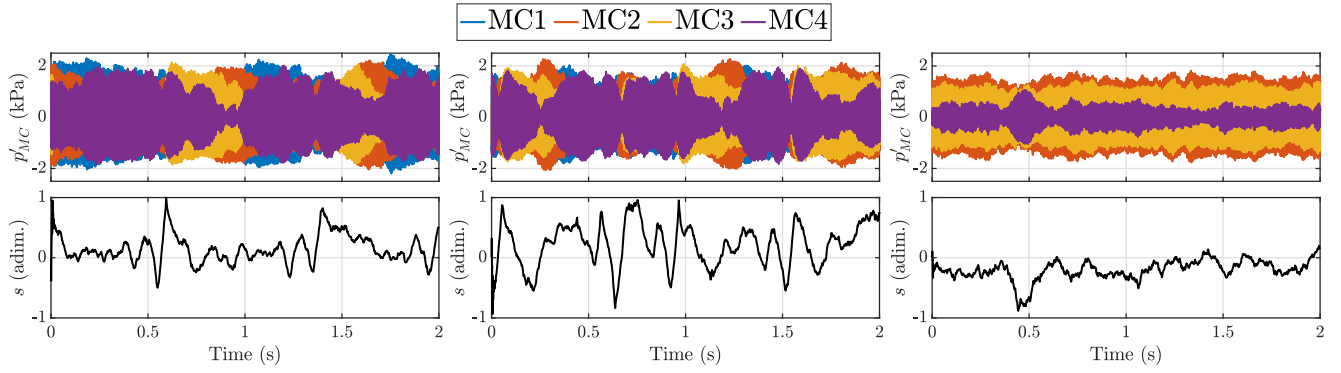


Fig. 4: Instability maps (MICCA-Spray) showing the amplitude (left) and frequency (right) of instability at different operating points (varying in  $\mathcal{P}$  and  $\phi$ ) for the three fuels. The measurements are performed at five thermal powers ( $\mathcal{P} \approx 93\text{ kW}, 99\text{ kW}, 103\text{ kW}, 110\text{ kW}, 118\text{ kW}$ ) and at each thermal power six equivalence ratios are considered ( $\phi = 0.75, 0.85, 0.9, 0.95, 1.0, 1.05$ ). The black star, blue diamond and black circle respectively correspond to operating points F-1 ( $\phi = 0.85$ ), F-2 ( $\phi = 0.95$ ) (both at  $\mathcal{P} = 6.4\text{ kW}$ ), and F-3 ( $\phi = 0.95$  and  $\mathcal{P} = 7.4\text{ kW}$ ) used for FDF measurements in SICCA-Spray (Tab. 1).

#### INSTABILITY MAPS OF MICCA-SPRAY

The instability maps of MICCA-Spray are determined from a total of thirty different operating points (in terms of

global equivalence ratio,  $\phi$ , and thermal power,  $\mathcal{P}$ ) for the three fuels. The fuel flow rate is fixed for each thermal power,



(a) Propane ( $\mathcal{A} \approx 1274\text{Pa}$  &  $f_{ins} = 813\text{Hz}$ ) (b) Heptane ( $\mathcal{A} \approx 1227\text{Pa}$  &  $f_{ins} = 813\text{Hz}$ ) (c) Dodecane ( $\mathcal{A} \approx 1065\text{Pa}$  &  $f_{ins} = 800\text{Hz}$ )

Fig. 5: A typical time evolution of MICCA-Spray chamber pressure signals and spin ratio at the same operating point ( $\mathcal{P} = 110\text{kW}$  and  $\phi = 0.9$ ) for the three fuels. The amplitude and frequency of instability are also indicated for each fuel at this operating point.

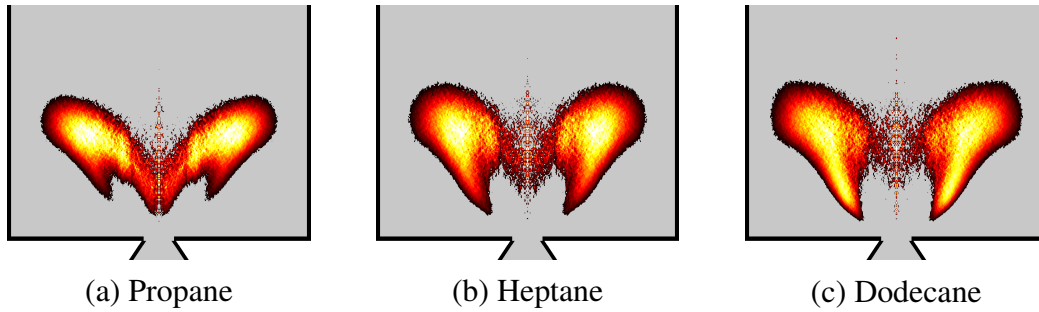


Fig. 6: SICCA-Spray flame images, corresponding to F-1 ( $\mathcal{P} = 6.4\text{kW}$ ,  $\phi = 0.85$ ), showing the chemiluminescence of  $\text{CH}^*$  captured using a PI-MAX camera with a gate delay of 5 ms. A single image is obtained by time accumulation of 30 frames and an Abel transform is applied to these images.

and the airflow rate is changed to sweep the range of global equivalence ratios or equivalently, the range of fuel-air ratios. The translation between global equivalence ratio to fuel-air ratio can be obtained by multiplying  $\phi$  by the fuel-air ratio at stoichiometric conditions,  $\kappa$ . The value of  $\kappa$  is 0.0641 for propane, 0.0662 for heptane, and 0.0669 for dodecane. Different acoustic instabilities may appear in the combustion chamber depending on the operating points. There may be 1L type longitudinal modes or 1A-1L type azimuthal-longitudinal modes as the combustion chamber is open to the atmosphere. In the present study, the operating conditions corresponding to 1L modes were not considered. The operating points examined gave only stable operation or 1A-1L modes. During an instability coupled by a 1A-1L azimuthal acoustic mode, the acoustic pressure signal near the combustor backplane can be represented by

$$p'(\theta, t) = A^+ \exp(i\theta - i\omega t) + A^- \exp(-i\theta - i\omega t) \quad (2)$$

Here,  $p'$  is the instantaneous pressure signal that can be obtained from the microphone measurements,  $A^+$  and  $A^-$  represent the amplitudes of counter-clockwise and clockwise spinning components of the 1A-1L azimuthal acoustic mode respectively, and  $\theta$  is the azimuthal angle as de-

finied in Fig. 1. From the reconstructed amplitude values of counter-clockwise and clockwise waves, it is possible to deduce an instability amplitude that is spatially averaged over eight microphone signals and temporally averaged over 16s recordings. This amplitude is proportional to the root mean square (RMS) amplitude averaged over the annular cross-section given in Vignat et al. [2] and is calculated as

$$\mathcal{A} = (|A^+|^2 + |A^-|^2)^{1/2} \quad (3)$$

$\mathcal{A}$  is an indicator of the level of instability that is independent of the structure of the acoustic mode and is used here as a metric to compare the instability behavior of MICCA-Spray with the three fuels. The individual wave amplitudes are determined from the pressure signals measured by the eight chamber microphones (MC1-MC8). The microphone signals are bandpass-filtered between 500Hz to 1100Hz and the time-resolved analytical signals are constructed using the Hilbert transform. The wave amplitudes are determined with the method developed by Vignat et al. [2] up to third order in azimuthal harmonics, for a better fidelity in terms of pressure field reconstruction. The amplitude calculated using Eq. (3) at various operating points are interpolated to derive instability maps for MICCA-Spray, as shown in Fig. 4

(left). Overall, in the operating regime considered, premixed propane features broader unstable regions with higher  $\mathcal{A}$  values (red & yellow shades). The maximum amplitude value  $\mathcal{A} \approx 1460$  Pa is reached at  $\mathcal{P} = 110$  kW and  $\phi = 0.85$ . Comparatively narrower regions of instability are found for heptane but its maximum amplitude is the highest among the three fuels,  $\mathcal{A} \approx 1670$  Pa and corresponds to  $\mathcal{P} = 110$  kW and  $\phi = 1.05$ . Dodecane exhibits the narrowest unstable region with a maximum amplitude  $\mathcal{A} \approx 1500$  Pa occurring at  $\mathcal{P} = 118$  kW and  $\phi = 0.9$ . At the lowest global equivalence ratio ( $\phi = 0.75$ ), the oscillation amplitude is low, indicating that the system is stable at this point irrespective of the fuel that is being used. For the lowest power ( $\mathcal{P} = 93$  kW), propane is mostly unstable, whereas the liquid fuels are always stable (indicated by blue regions). For a given power ( $\mathcal{P} = 110$  kW), propane features a high level of oscillation at a leaner point ( $\phi = 0.9$ ), while heptane exhibits a maximum level at a richer condition ( $\phi = 1.05$ ). Such a trend is not observed for dodecane. In summary, the instability maps indicate that, in the operating conditions considered, the system is most unstable when operated with premixed propane and air, followed by heptane and then dodecane, and the extent of the instability region narrows down as the time delay associated with liquid fuel atomization and vaporization is augmented.

The frequency of instability is deduced from the power spectral densities of pressure signals, which are calculated by averaging  $M = 64$  periodograms using Hamming windows of  $N = 4096$  data samples with 50% overlap. Each window contains data for 0.25 s resulting in a frequency resolution  $\Delta f = 4$  Hz. The interpolated frequency map is shown in Fig. 4 (right). Propane has a maximum frequency value of 840 Hz followed by heptane which has a slightly lower peak frequency at 816 Hz. Dodecane has the lowest maximum frequency value of 808 Hz.

It is next interesting to examine the spin ratio corresponding to the three fuel injection conditions. This ratio defined in [23] is deduced from the wave amplitudes as

$$s = (|A^+| - |A^-|) / (|A^+| + |A^-|) \quad (4)$$

Its value is such that when  $s = 0$ , the mode is standing while  $s = 1$  or  $s = -1$  represents a spinning mode in counter-clockwise or clockwise directions respectively. A point is chosen on the instability map ( $\mathcal{P} = 110$  kW and  $\phi = 0.9$ ) where the three fuels have nearly the same amplitude to present the typical pressure signals from the four chamber microphones (MC1-MC4) and the temporal evolution of spin ratio (Fig. 5). It should be noted that, for the same operating point, the adiabatic temperatures and laminar burning velocities are very close for the three fuels, if all the fuels can be considered perfectly prevaporized and premixed with air during chemical conversion [28]. From the pressure signals, it can be seen that the oscillation is nearly at a limit cycle. One also finds that the spin ratio time series corresponding to the three fuels differ from each other, showing that the nature of the azimuthal modes coupling the oscillations is influenced

Table 1: Three operating conditions for FDF measurement in SICCA-Spray. The bulk velocity  $u_b$ , at the injector outlet, is calculated in cold flow conditions as  $u_b = \dot{m}_{\text{air}} / (\pi r_{\text{inj}}^2 \rho_{\text{air}})$ .

Operating point	$\mathcal{P}$	$\phi$	$\dot{m}_{\text{air}}$	$u_b$
	(kW)	(-)	(g s <sup>-1</sup> )	(m s <sup>-1</sup> )
F-1	6.4	0.85	2.6	43
F-2	6.4	0.95	2.3	38
F-3	7.4	0.95	2.6	43

by the fuel type, an intriguing feature that needs further investigation.

## FLAME DESCRIBING FUNCTION MEASUREMENTS

The instabilities observed in MICCA-Spray can be further explained by measuring the response of a single flame to acoustic perturbations. As already indicated, the FDF measurements are performed in SICCA-Spray at three operating points (shown in Tab. 1): two points at  $\mathcal{P} \approx 6.4$  kW and at an equivalence ratio of  $\phi = 0.85$  and  $\phi = 0.95$  (henceforth referred to as F-1 and F-2 respectively), corresponding to a thermal power of 103 kW in MICCA-Spray; and a third point at  $\mathcal{P} \approx 7.4$  kW and at an equivalence ratio of  $\phi = 0.95$  (henceforth referred to as F-3), corresponding to a thermal power of 118 kW in MICCA-Spray (see Fig. 4). Normally, for the FDF measurements, the chamber length in SICCA-Spray is fixed at  $l_{\text{chamber}} = 165$  mm except at F-3 point wherein the measurements are performed with a length  $l_{\text{chamber}} = 115$  mm, as SICCA-Spray exhibits mild self-sustained instability with  $l_{\text{chamber}} = 165$  mm at F-3. In order to verify that the FDF results do not depend on the chamber length, a separate measurement was performed with  $l_{\text{chamber}} = 115$  mm at the F-1 operating point. This measurement produced the same results at both 165 mm and 115 mm, thus indicating that the FDFs do not depend on the chamber length as long as the system is not exhibiting any self-sustained instabilities. The flame images at F-1, displayed in Fig. 6, show the differences in flame shape between premixed and spray flames. In the case of propane, the flame is full “M”-shaped, and for heptane and dodecane, it is a hollow “M” with a central trough. The spray conveys the fuel outwards, and there is a relative absence of fuel close to the injector axis. This favors a hollow “M”-flame for liquid fuel injection. However, in the case of propane and air, the reaction can take place in the inner shear layer because the fresh mixture in this region has a suitable equivalence ratio to burn, resulting in a full “M”-flame. The flame shapes at F-2 and F-3 (not shown here) are similar to the ones shown in Fig. 6 for all the three fuels.

The FDF provides the nonlinear response of the flame to

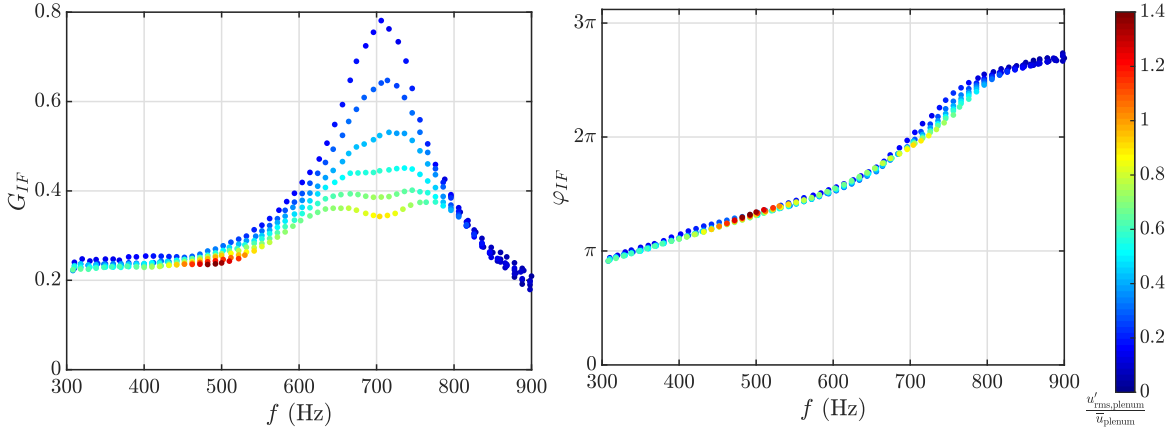


Fig. 7: FDF (gain and phase) results for measurements performed in SICCA-Spray for propane at F-1 ( $\mathcal{P} = 6.4\text{kW}$  &  $\phi = 0.85$ ) with color axis representing the level of velocity fluctuations  $u'_{\text{rms,plenum}}/\bar{u}_{\text{plenum}}$  in the plenum. Here,  $u'_{\text{rms,plenum}}$  is the RMS velocity fluctuations calculated using the two microphone method and  $\bar{u}_{\text{plenum}}$  is the bulk velocity in the plenum at MP2 location (Fig. 2). The FDFs shown here include the response of the flame as well as the injection system dynamics (denoted by the subscript IF).

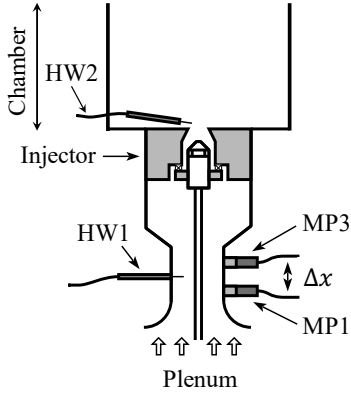


Fig. 8: Schematic of the experimental setup used for measuring the injector describing function in SICCA-Spray. The measurements are performed under cold flow conditions. Only a part of the plenum is shown in this drawing. See Fig. 2 for a full view of the system.

the incoming acoustic velocity perturbation and is given by

$$\mathcal{F}(\omega, |u'|) = \frac{\dot{Q}'(\omega, |u'|)/\bar{Q}}{u'/\bar{u}} = G(\omega, |u'|)e^{i\phi(\omega, |u'|)} \quad (5)$$

Here,  $G = |\mathcal{F}|$  and  $\phi = \arg(\mathcal{F})$  are the gain and phase of the FDF.  $\dot{Q}'$ , the fluctuation in heat release rate (HRR), and  $\bar{Q}$ , the mean HRR, are deduced from the light intensity of  $\text{OH}^*$ ,  $u'$  is the acoustic velocity fluctuation determined from the two microphone technique,  $\bar{u}$  is the bulk velocity that is calculated from the mass flow rate and cross-sectional area in the hot wire section (Fig. 2).  $\bar{u}$  has a value of approximately  $2.7\text{ m s}^{-1}$  at F-1 & F-3, and  $2.4\text{ m s}^{-1}$  at F-2 for liquid fuels and  $2.9\text{ m s}^{-1}$  at F-1 & F-3, and  $2.6\text{ m s}^{-1}$  at F-2 for premixed propane.

As mentioned earlier, different levels of velocity fluctu-

ation are obtained during the frequency sweep at a rate of  $4.5\text{ Hz s}^{-1}$  for different voltage levels ( $V_0$ ) of a function generator, resulting in various levels of  $u'/\bar{u}$ . During the frequency sweep, the measurement channels are scanned by blocks of 32,768 points at the rate of  $f_s = 16,384\text{ Hz}$ , resulting in a total time duration of 2 s for a particular modulation frequency  $f$ . The transfer function is obtained using Welch's periodogram method to calculate the cross-power spectral density between  $u'$  and  $\dot{Q}'$ . Each 2 s signal is divided into 8 segments with Hamming windows and 50% overlap to obtain the gain  $G(f)$  and phase  $\phi(f)$  of the transfer function at  $f$ . Figure 7 shows the gain and phase of the FDF for different levels of input velocity fluctuations for propane. It is important to note that for these FDF plots, the acoustic velocity fluctuations are calculated in the plenum, meaning that the transfer function includes the effect of the flame in combination with the injector dynamical response (indicated by a subscript IF).

The inclusion of injector dynamics in FDF introduces an injector phase  $\phi_I$  and gain  $G_I$  that needs to be corrected in the FDF measurements. To measure this, two hot wires are used, one in the plenum (HW1—measuring  $u'_1$ ) and another at a height of 2.5 mm above the backplane and at a distance of 3 mm from the axis of the injector (HW2—measuring  $u'_2$ ), as shown in Fig. 8. The measurements to obtain the injector describing functions were performed under cold flow conditions with  $l_{\text{chamber}} = 165\text{ mm}$ . It has been found from numerical simulations with LES [37] that, at this location, the relative velocity fluctuations are equivalent (both in phase and gain) to the relative mass flow rate fluctuations. A frequency sweep (same as for FDF-IF measurements) with varying levels of amplitude was performed, and the velocities from the two hot wires were measured. Figure 9 shows the variation of  $G_I$  and  $\phi_I$  with respect to frequency for the various loudspeaker forcing voltages. From the figure, it can be seen that the value of the gain changes when the amplifier voltage is different but the value of the phase only features small varia-

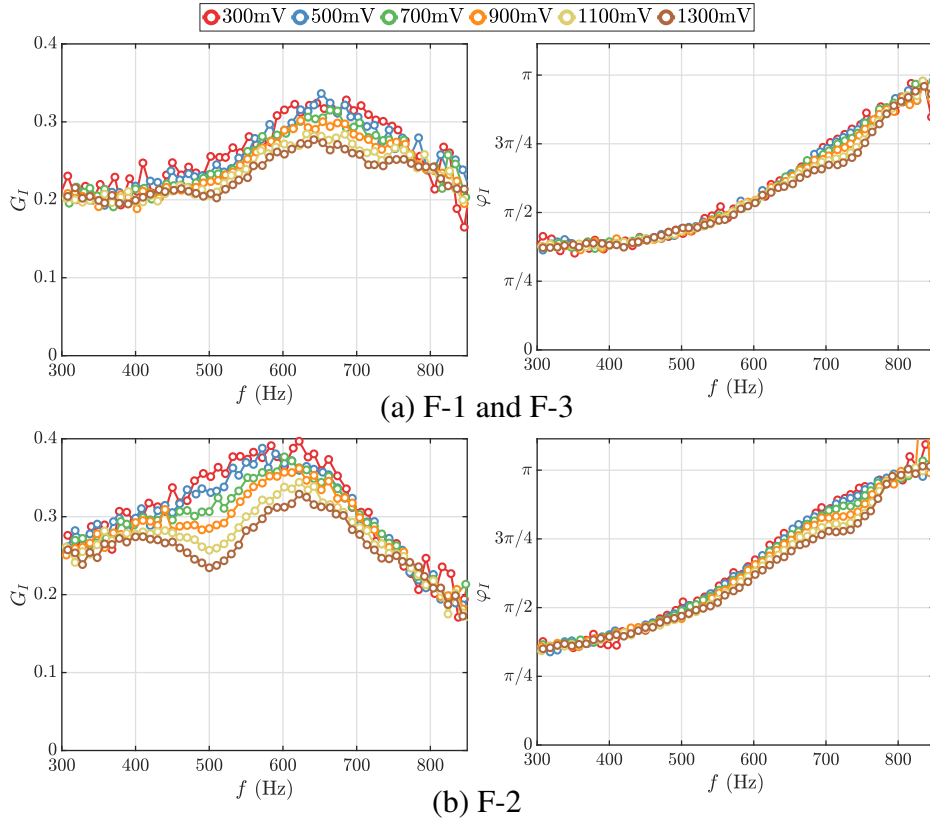


Fig. 9: Evolution of gain and phase between the velocity measured in the plenum ( $u_1'$  from HW1 (Fig. 8)) and at the injector outlet ( $u_2'$  from HW2) with respect to frequency, for different loudspeaker excitation voltages. The measurement is carried out at two airflow rates that correspond to F-1 and F-3 (air at  $2.6 \text{ g s}^{-1}$  at the top) & F-2 (air at  $2.3 \text{ g s}^{-1}$  in the bottom).

tions with amplifier voltage. Using these measurements, the describing function considering only the flame response to acoustic perturbations is obtained as follows:

$$G_F = \frac{G_{IF}}{G_I} \quad \& \quad \varphi_F = \varphi_{IF} - \varphi_I \quad (6)$$

The plots in Fig. 10 corresponding to the three fuels at F-1 indicate that the gain  $G_F$  changes substantially with the amplitude of the incident fluctuations and features a maximum at a frequency  $f_{\text{peak}}$  for the three fuels. For propane, this peak is prominent only in the linear regime at low velocity fluctuation levels. The peak frequency shifts to lower values as one moves from propane to heptane and then to dodecane. The gain decreases with amplitude showing a nonlinearity. On the contrary, there is almost no change in the phase  $\varphi_F(f)$  at different excitation levels. This kind of evolution has been classically observed with “M”-flames [38]. The phase curves are roughly linear until the point where the gain begins to increase. After this point, the slope of the phase curves increases slightly. This may be related to a convective motion of the perturbations with large structures created at the injector outlet and moving at lower speed compared to the small perturbations at the flame foot. For the FDF results at F-2 and F-3 operating points, the readers are referred to the supplementary material.

Figure 11 shows the FTF gain and phase at the three measurement points at the lowest excitation amplitude ( $V_0 = 300 \text{ mV}$ ). The value of  $f_{\text{peak}}$  does not change with the change in global equivalence ratio  $\phi$  (red and black curve) but increases to a higher frequency with the change in  $\mathcal{P}$  (for the same equivalence ratio, shown by black and blue curve). Between F-1 and F-2 points, the gain for all the three fuels close to  $f_{\text{peak}}$  is lower at F-2 compared to F-1. Between F-2 and F-3, the gain value close to  $f_{\text{peak}}$  for the three fuels at F-3 is higher than at F-2.

It is interesting to extract time delays from the phase plots of the FDFs. This may be accomplished in general by taking the derivative of the phase with respect to the angular frequency as  $\tau_{u'_i - \dot{Q}'} = d\varphi_{u'_i - \dot{Q}'} / d\omega$ . It can be seen in Fig. 12 that the phase shifts are in increasing order, first the premixed propane, then the heptane with a greater phase shift, and then dodecane, which can, in-turn be attributed to different time lags. For premixed propane, the associated time lags will just be the time taken by the reactants to reach the combustion zone, i.e., convection time delay  $\tau_{\text{conv}}$  and the delay associated with the chemical processes involved in combustion  $\tau_{\text{reac}}$ . On the other hand, when liquid fuels are used, additional time-lags due to atomization  $\tau_{\text{atm}}$ , vaporization  $\tau_{\text{vap}}$ , and mixing  $\tau_{\text{mix}}$  need to be considered. The case of heptane is likely to be close to propane, wherein the vaporization could be happening simultaneously with convection [9,20].

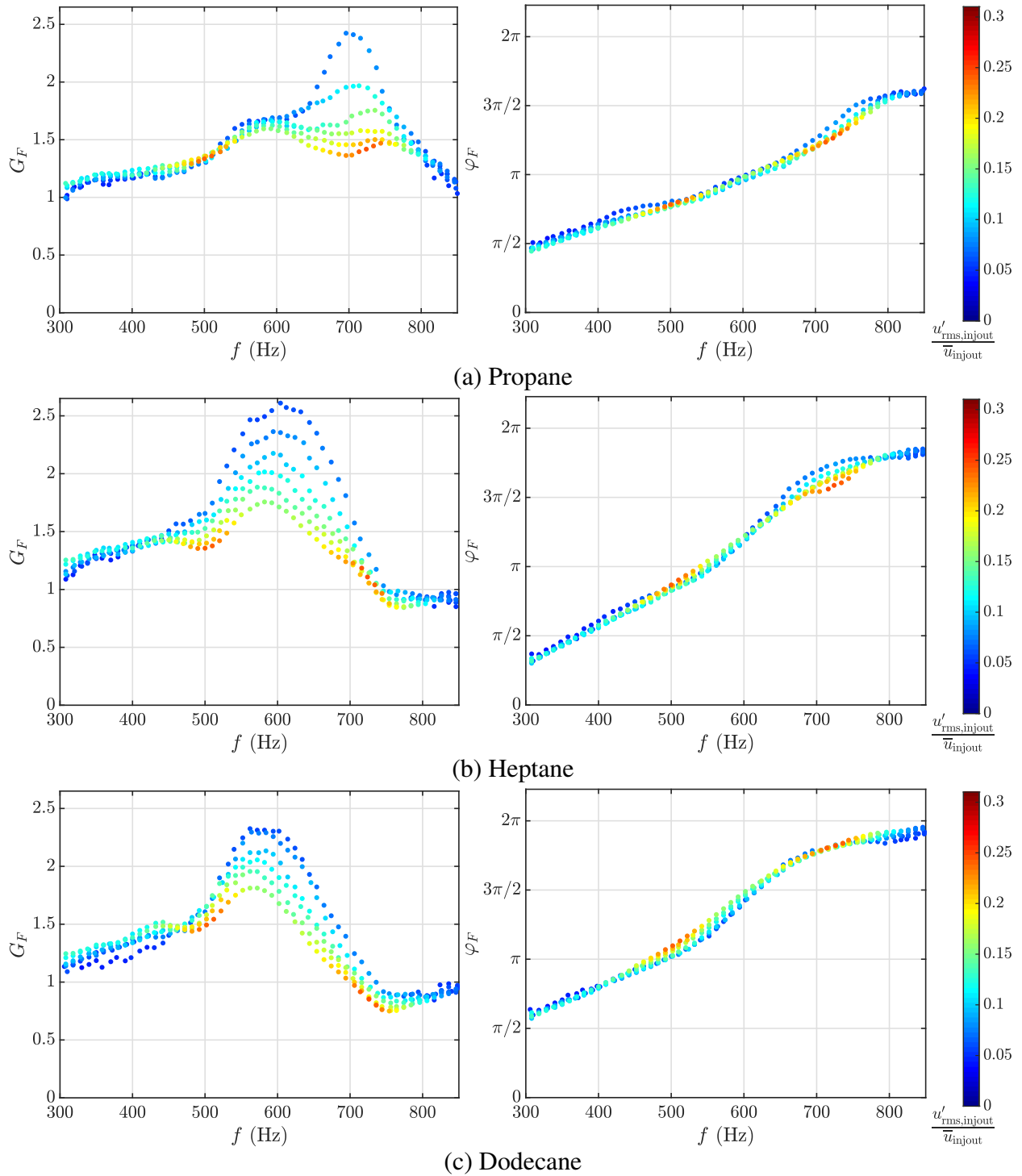


Fig. 10: FDF (gain  $G_F$  and phase  $\phi_F$ ) of flame obtained after correcting for the injector describing function (Eq. (6)) in SICCA-Spray for the three fuels at F-1 ( $\mathcal{P} = 6.4 \text{ kW}$  &  $\phi = 0.85$ ) with color axis representing the level of velocity fluctuations  $u'_{\text{rms},\text{injout}}/\bar{u}_{\text{injout}}$  at the injector outlet (injout). Here,  $u'_{\text{rms},\text{injout}}$  is the RMS velocity fluctuations from HW2 and  $\bar{u}_{\text{injout}}$  is the mean of HW2 (refer to Fig. 8 for HW2 location). These FDFs represent the flame response to acoustic perturbations. The data are smoothed using a five-point moving average.

However, for the case of dodecane, due to its lower volatility, the situation is likely to be dominated by the time delay associated with vaporization. A change of slope is observed in the phase curves at around 550Hz. This change of slope

appears when the gain moves towards its maximum value. It is likely that the disturbances created on the flame front grow in magnitude and travel at a slower speed. The FDF data set reported in this section will now be used together with the

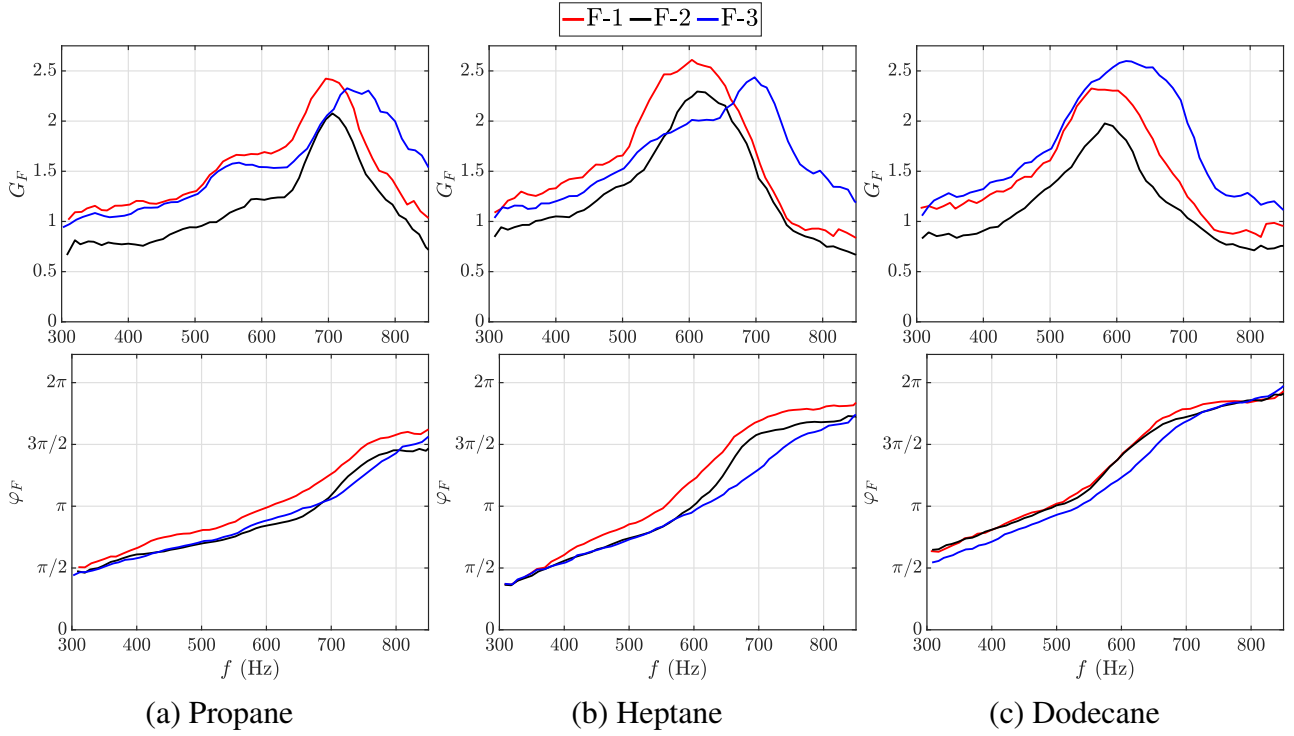


Fig. 11: FTF (gain  $G_F$  and phase  $\varphi_F$ ) results for measurements performed in SICCA-Spray for the three fuels at the lowest excitation voltage  $V_0 = 300$  mV. Red, black and blue colors correspond to the measurements at F-1, F-2, and F-3 operating points. The values in the plots are smoothed using a five-point moving average.

oretical results to interpret the instability behavior observed in the annular combustor, MICCA-Spray.

### LINK BETWEEN THE INSTABILITIES IN THE ANNULAR COMBUSTOR AND FDF MEASUREMENTS

An attempt is now made to link observations in MICCA-Spray and FDF measurements in SICCA-Spray. It is first convenient to gather the amplitude and frequency of oscillation observed in MICCA-Spray at the same operating conditions as FDF measurements (F-1, F-2 & F-3). These data are summarized in Tab. 2. One may next try to infer the bands of instability from theory. This can be done by making use of an instability analysis in which the flames formed by the injectors can be treated as compact with respect to the wavelength. This analysis carried out in [39] consists of unwrapping the annular combustor as an equivalent rectangular system and applying periodic boundaries on the lateral walls. One may then derive a dispersion relation and obtain an estimate of the growth rate  $\omega_i$ . For a mixed  $(m+1)A-(n+1)L$  azimuthal-longitudinal mode, the growth rate of acoustic oscillations is

$$\omega_i = -(-1)^n \frac{k_x^n}{k_m^n} \sin\left((2n+1)\frac{\pi a}{2l}\right) \sin\left((2n+1)\frac{\pi b}{2l}\right) \frac{c}{l} \Theta G_F(\omega_m^n) \sin(\varphi_F(\omega_m^n)) \quad (7)$$

Here,  $k_x^n$  is the axial wavenumber and  $k_m^n = 2\pi c f_m^n$ , where  $f_m^n$  is the frequency of instability. The flames are assumed to be located at a distance  $a$  from the chamber backplane,  $b$  is the distance from the flame location to the end of the chamber and  $l = a + b$ .  $c$  is the speed of sound, and  $\Theta = T_2/T_1 - 1$  represents the temperature jump across the flame.  $G_F$  and  $\varphi_F$  are the gain and phase of FDF at the angular frequency of instability,  $\omega_m^n$ . For a 1A-1L mode ( $m = 0$  and  $n = 0$ ), the growth rate of oscillation  $\omega_i \propto -G_F(\omega_0^0) \sin(\varphi_F(\omega_0^0))$ . This product will be designated in what follows as the instability index  $\Gamma$ .

The sign of  $\Gamma$  defines the bands where the annular combustor is linearly unstable for the 1A-1L mode. The system can be classified to be unstable if  $\omega_i > 0$ , that is, when  $\Gamma = -G_F \sin(\varphi_F)$  is positive, which corresponds to  $\pi < \varphi_F < 2\pi \pmod{2\pi}$  [39–41]. This defines the unstable bands in the phase diagram of FDF (gray bands in Fig. 12). Note that the figure only shows the first band extending from  $\pi$  to  $2\pi$ . These bands represent the frequency range within which the system can be unstable. The instability frequencies in MICCA-Spray (Tab. 2) can then be compared with the bands delimited in Fig. 12. Based on whether or not the instability frequency,  $f_{\text{ins}}$  of MICCA-Spray lies within these unstable bands marked on the FDF, the stability of the system can be determined. In Fig. 12, the  $f_{\text{ins}}$  of MICCA-Spray are denoted by diamond markers and color-coded by the fuel. Notably, this criterion provides a necessary but not a sufficient condition for instability. That is, if the instability frequency lies

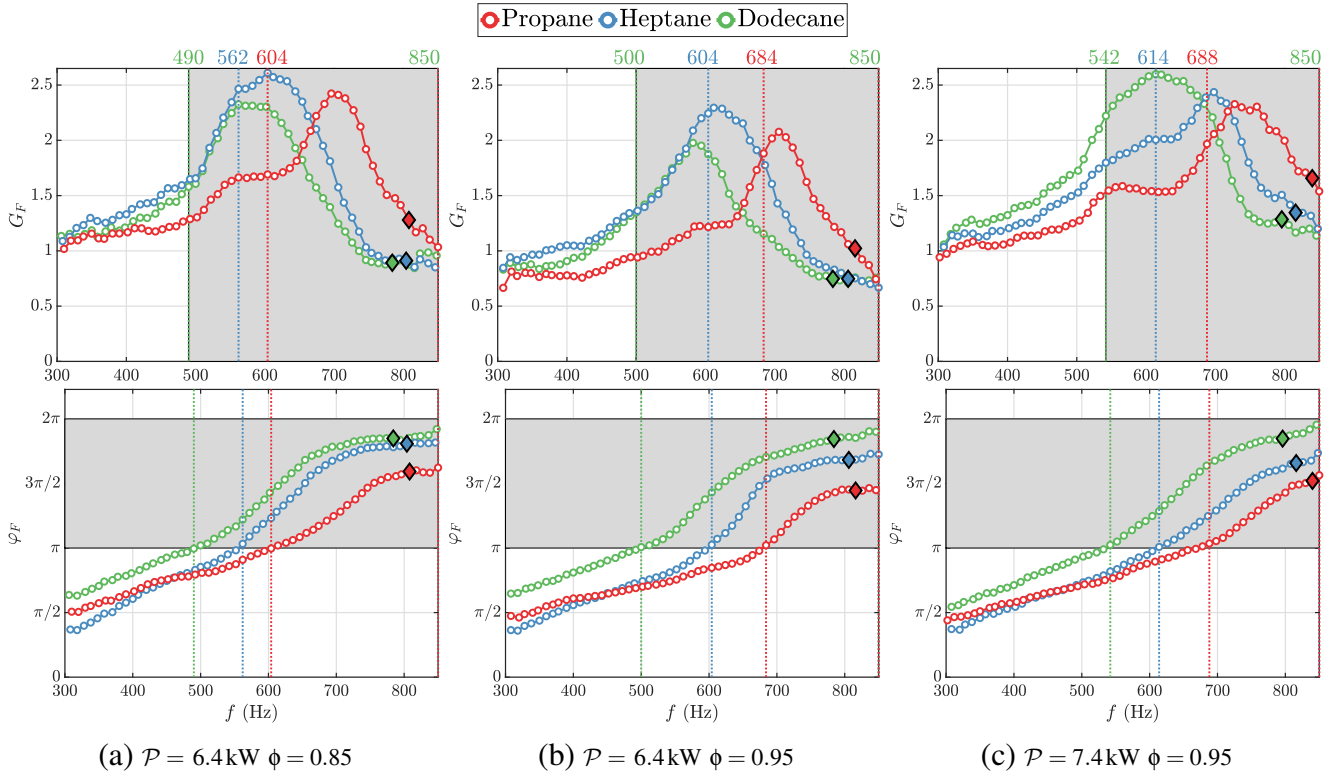


Fig. 12: FTF for the three fuels at  $V_0 = 300\text{mV}$  ( $u'_{\text{rms, injout}}/\bar{u}_{\text{injout}} = 0.04$  to  $0.12$ ) and at F-1 ( $\mathcal{P} = 6.4\text{kW}, \phi = 0.85$ ), F-2 ( $\mathcal{P} = 6.4\text{kW}, \phi = 0.95$ ) and F-3 ( $\mathcal{P} = 7.4\text{kW}, \phi = 0.95$ ). Gray bands represent the unstable regions and the red, blue and green vertical dotted lines bounding the gray bands represent the instability limits for propane, heptane and dodecane respectively. The frequency limits (in Hz) of the unstable bands are marked on the plots at the top and the diamond markers indicate the MICCA-Spray instability frequency at the respective operating points (refer to Tab. 2), color-coded by the type of fuel. The data shown have been smoothed using a five-point moving average.

Table 2: Amplitude and frequency of instability in MICCA-Spray at the operating points F-1, F-2, and F-3. The instability index  $\Gamma$ , which is calculated at the instability frequency with FDF data at the lowest excitation level  $V_0 = 300\text{mV}$  is also listed in the table.

		F-1	F-2	F-3
Propane	$\mathcal{A}$ (Pa)	1302	1156	814
	$f_{\text{ins}}$ (Hz)	800	816	836
	Instability index, $\Gamma$	1.35	1.12	1.52
		Highly unstable	Highly unstable	Unstable
Heptane	$\mathcal{A}$ (Pa)	795	1398	1241
	$f_{\text{ins}}$ (Hz)	800	808	813
	Instability index, $\Gamma$	0.63	0.64	1.38
		Unstable	Highly unstable	Highly unstable
Dodecane	$\mathcal{A}$ (Pa)	548	285	608
	$f_{\text{ins}}$ (Hz)	784	781	799
	Instability index, $\Gamma$	0.39	0.35	0.59
		Unstable	Mildly unstable	Unstable

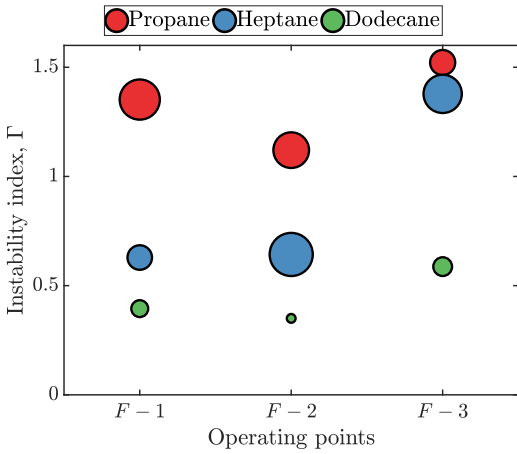


Fig. 13: Values of the instability index at each operating point for the three fuels. Color of the markers correspond to the fuel while the marker size is proportional to the amplitude of instability observed in MICCA-Spray.

outside this band, it corresponds to a linearly stable operation of MICCA-Spray. Whereas, if the instability frequency lies inside this band, it does not certainly mean that the system will be unstable. In addition to knowing whether the phase of FDF lies inside this band, it is also important that the growth rate  $\omega_i$  be larger than the damping rate in the system, which requires knowing the value of the instability index  $\Gamma$ .

The instability index can then be used as a metric to predict the instability of the annular system based on the gain and phase of FDF. The value of the instability index calculated with the linear range of FDF ( $V_0 = 300$  mV) at the frequency of instability of MICCA-Spray ( $f_{ins}$ ) is tabulated in Tab. 2 and shown in Fig. 13 for the operating conditions considered in this study. In all the cases, the value of  $\Gamma$  is positive, indicating that the MICCA-Spray annular combustor may linearly be unstable at all these points. Interestingly, the lowest value of the instability index corresponds to F-2 for dodecane (smallest circle in Fig. 13), and this point only features a mild instability in MICCA-spray. In general, it can be observed that a higher value of the instability index corresponds to a higher level of instability amplitude in MICCA-Spray. However, at F-2 and F-3, even though propane has a higher instability index than heptane, the level of instability in MICCA-Spray is higher for heptane than propane. This is because the instability index is derived from linear instability theory while the oscillations in the annular combustor are observed at limit cycle and therefore depend on the nonlinear response of the flame and the value of the damping rate.

It is also important to note that the single injector conditions in SICCA-Spray are not exactly the same as those found in the MICCA-Spray annular combustor. For instance, in MICCA-Spray, each flame is adjacent to other flames resulting in burnt gas interactions that might possibly change the flame dynamics ([42,43]). Also, the injector response measurements are carried out 2.5 mm above the injector outlet under cold flow conditions. The presence of flame can slightly modify the velocity profile. Furthermore, the injec-

tor impedance is not accounted for in this analysis. For the points considered at the limit of the instability bands, there may be some uncertainty as to whether the annular chamber will feature an instability or not. In addition, if the frequency of the resonant mode is changed by modifying the geometry of MICCA-Spray (for example, by changing the chamber length), the system could be more unstable for liquid fuels than for premixed propane. The FDFs are studied in SICCA-Spray using longitudinal forcing only and some flames in MICCA-Spray are simultaneously submitted to transverse velocity fluctuations as well due to the azimuthal mode structures. Nevertheless, the previous analysis helps in gaining a general understanding of the instabilities in annular systems.

## CONCLUSION

This article is mainly focused on the influence of fuel properties and physical state on thermo-acoustic instabilities coupled with azimuthal modes. The changes in fuel have a direct impact on the time lag. The shortest time lag corresponds to premixed propane and air. The time lag is augmented for heptane and takes its largest values for the less volatile dodecane. A database is obtained from systematic experiments on a laboratory-scale annular combustor (MICCA-Spray) for a wide range of operating points that vary in thermal power and global equivalence ratio. Results show that the largest instability domain is obtained for premixed propane. In comparison, the instability contour shrinks in the case of heptane, revealing a larger stable region. The stability of the system is further augmented when it is operated with dodecane. Thus, in this case, having a fuel which has a higher time lag makes the system more stable. A difference between the three fuels can be observed in the frequency of oscillation as well. At a point where the three fuels have nearly the same oscillation amplitude levels, it is found that propane and heptane have the same instability frequency, while dodecane features a lower instability frequency. An attempt is made to understand this dynamic behavior using flame describing function (FDF) measurements in a single sector configuration at three operating points in the instability map. The FDF phase plots are used to define unstable bands and an instability index is obtained by combining the gain and phase of FDF at each operating condition. In general, when the instability index is positive, which in turn corresponds to oscillation frequency being within the unstable band of the phase plots, the annular combustor is unstable. Overall, if the value of the instability index is high, one finds that the amplitude of oscillation in MICCA-Spray is large. However, this observation does not extend to few operating conditions and one cannot expect to have a monotonic relation because the instability band and index are defined in the linear regime while the observations in the annular combustor are made at the limit cycle. Also, the FDFs are measured in a single injector setup with a flame that is not exactly in the same environment as the flames in the annular chamber. Nevertheless, the single sector FDF measurements can be effectively used to interpret instability experiments in multiple injector annular combustor systems.

## Acknowledgements

This work was supported by SafranTech (contract NF5Z-5100), project FASMIC ANR16-CE22-0013 of the French National Research Agency (ANR), and European Union's Horizon 2020 research and innovation program, Anulight with grant agreement no. 765998.

## References

- [1] Prieur, K., Durox, D., Schuller, T., and Candel, S., 2018. "Strong azimuthal combustion instabilities in a spray annular chamber with intermittent partial blow-off". *J. Eng. Gas Turb. Power*, **140**(3), p. 031503.
- [2] Vignat, G., Durox, D., Renaud, A., and Candel, S., 2020. "High Amplitude Combustion Instabilities in an Annular Combustor Inducing Pressure Field Deformation and Flame Blow Off". *J. Eng. Gas Turb. Power*, **142**(January), p. 011016.
- [3] Huang, Y., and Yang, V., 2009. "Dynamics and stability of lean-premixed swirl-stabilized combustion". *Prog. En. & Comb. Sc.*, **35**(4), pp. 293–364.
- [4] Candel, S., Durox, D., Schuller, T., Bourgouin, J.-F., and Moeck, J. P., 2014. "Dynamics of swirling flames". *Annual Rev. of Fluid Mech.*, **46**, pp. 147–173.
- [5] Poinot, T., 2017. "Prediction and control of combustion instabilities in real engines". *Proc. Combust. Inst.*, **36**(1), pp. 1–28.
- [6] Eckstein, J., Freitag, E., Hirsch, C., and Sattelmayer, T., 2006. "Experimental study on the role of entropy waves in low-frequency oscillations in a rql combustor". *J. Eng. Gas Turb. Power*, **128**(2), pp. 264–270.
- [7] Gajan, P., Strzelecki, A., Platet, B., Lecourt, R., and Giuliani, F., 2007. "Investigation of spray behavior downstream of an aeroengine injector with acoustic excitation". *J. Prop. Power*, **23**(2), pp. 390–397.
- [8] Kim, W., Zhang, S., Palies, P., Cohen, J., Liljenberg, S., and Hautman, D., 2012. "The behavior of liquid fuel sprays in acoustically-forced air swirler flows". In ASME Turbo Expo 2012, no. GT2012-68922.
- [9] Vignat, G., Lo Schiavo, E., Laera, D., Renaud, A., Gicquel, L., Durox, D., and Candel, S., 2021. "Dynamics of spray and swirling flame under acoustic oscillations: A joint experimental and LES investigation". *Proc. Combust. Inst.*, **000**, pp. 1–10.
- [10] Lo Schiavo, E., Laera, D., Riber, E., Gicquel, L. Y., and Poinot, T., 2020. "Effects of liquid fuel/wall interaction on thermoacoustic instabilities in swirling spray flames". *Combust. Flame*, **219**, pp. 86–101.
- [11] Pillai, A. L., Nagao, J., Awane, R., and Kurose, R., 2020. "Influences of liquid fuel atomization and flow rate fluctuations on spray combustion instabilities in a backward-facing step combustor". *Combust. Flame*, **220**, pp. 337–356.
- [12] Rayleigh, L., 1878. "The explanation of certain acoustical phenomena". *Roy. Inst. Proc.*, **8**, pp. 536–542.
- [13] Crocco, L., 1951. "Aspects of combustion stability in liquid propellant rocket motors part I: fundamentals. low frequency instability with monopropellants". *J. Am. Rocket Soc.*, **21**(6), pp. 163–178.
- [14] Crocco, L., 1952. "Aspects of combustion stability in liquid propellant rocket motors part II: Low frequency instability with bipropellants. high frequency instability". *J. Am. Rocket Soc.*, **22**(1), pp. 7–16.
- [15] Lee, J.-Y., Lubarsky, E., and Zinn, B. T., 2005. "Slow active control of combustion instabilities by modification of liquid fuel spray properties". *Proc. Combust. Inst.*, **30**(2), pp. 1757–1764.
- [16] Yu, K., Wilson, K., and Schadow, K., 1998. "Liquid-fueled active instability suppression". In Symp. (Intl.) Comb., Vol. 27, Elsevier, pp. 2039–2046.
- [17] Zhu, M., Dowling, A., and Bray, K., 1999. "Combustion oscillations in burners with fuel spray atomisers". In ASME 1999, Int. Gas Turb. & Aeroengine Cong. & Exb., no. 99-GT-302.
- [18] Apeloig, J. M., d'Herbigny, F.-X., Simon, F., Gajan, P., Orain, M., and Roux, S., 2014. "Liquid-fuel behavior in an aeronautical injector submitted to thermoacoustic instabilities". *J. Prop. Power*, **31**(1), pp. 309–319.
- [19] Tachibana, S., Saito, K., Yamamoto, T., Makida, M., Kitano, T., and Kurose, R., 2015. "Experimental and numerical investigation of thermo-acoustic instability in a liquid-fuel aero-engine combustor at elevated pressure: Validity of large-eddy simulation of spray combustion". *Combust. Flame*, **162**(6), pp. 2621–2637.
- [20] Bernier, D., Lacas, F., and Candel, S., 2004. "Instability mechanisms in a premixed prevaporized combustor". *J. Prop. Power*, **20**(4), pp. 648–656.
- [21] Worth, N. A., and Dawson, J. R., 2013. "Modal dynamics of self-excited azimuthal instabilities in an annular combustion chamber". *Combust. Flame*, **160**(11), pp. 2476–2489.
- [22] Worth, N. A., and Dawson, J. R., 2013. "Self-excited circumferential instabilities in a model annular gas turbine combustor: Global flame dynamics". *Proc. Combust. Inst.*, **34**(2), pp. 3127–3134.
- [23] Bourgouin, J.-F., Durox, D., Moeck, J., Schuller, T., and Candel, S., 2015. "A new pattern of instability observed in an annular combustor: The slanted mode". *Proc. Combust. Inst.*, **35**(3), pp. 3237–3244.
- [24] Wolf, P., Staffelbach, G., Roux, A., Gicquel, L. Y., Poinot, T., and Moureau, V., 2009. "Massively parallel LES of azimuthal thermo-acoustic instabilities in annular gas turbines". *CR Mécanique*, **337**(6-7), pp. 385–394.
- [25] Staffelbach, G., Gicquel, L., Boudier, G., and Poinot, T., 2009. "Large eddy simulation of self excited azimuthal modes in annular combustors". *Proc. Combust. Inst.*, **32**(2), pp. 2909–2916.
- [26] Bauerheim, M., Cazalens, M., and Poinot, T., 2015. "A theoretical study of mean azimuthal flow and asymmetry effects on thermo-acoustic modes in annular combustors". *Proc. Combust. Inst.*, **35**(3), pp. 3219–3227.
- [27] Ghirardo, G., and Juniper, M. P., 2013. "Azimuthal instabilities in annular combustors: standing and spin-

- ning modes”. *Proc. R. Soc. Lond. A*, **469**(2157), p. 20130232.
- [28] Prieur, K., Durox, D., Beaunier, J., Schuller, T., and Candel, S., 2017. “Ignition dynamics in an annular combustor for liquid spray and premixed gaseous injection”. *Proc. Combust. Inst.*, **36**(3), pp. 3717–3724.
- [29] Dowling, A. P., 1997. “Nonlinear self-excited oscillations of a ducted flame”. *J. Fluid Mech.*, **346**, pp. 271–290.
- [30] Noiray, N., Durox, D., Schuller, T., and Candel, S., 2008. “A unified framework for nonlinear combustion instability analysis based on the flame describing function”. *J. Fluid Mech.*, **615**, pp. 139–167.
- [31] Palies, P., Durox, D., Schuller, T., and Candel, S., 2011. “Nonlinear combustion instability analysis based on the flame describing function applied to turbulent premixed swirling flames”. *Combust. Flame*, **158**(10), pp. 1980–1991.
- [32] Boudy, F., Durox, D., Schuller, T., Jomaas, G., and Candel, S., 2011. “Describing function analysis of limit cycles in a multiple flame combustor”. *J. Eng. Gas Turb. Power*, **133**(6), p. 061502.
- [33] Price, R., Hurle, I., and Sugden, T., 1969. “Optical studies of the generation of noise in turbulent flames”. In *Symp. (Intl.) Comb.*, Vol. 12, pp. 1093–1102.
- [34] Mirat, C., Durox, D., and Schuller, T., 2014. “Analysis of the spray and transfer function of swirling spray flames from a multi-jet steam assisted liquid fuel injector”. In *ASME Turbo Expo 2014*, no. GT2014-25111.
- [35] Chung, J., and Blaser, D., 1980. “Transfer function method of measuring in-duct acoustic properties. I. theory”. *J. Acous. Soc. America*, **68**(3), pp. 907–913.
- [36] Seybert, A. F., and Ross, D. F., 1977. “Experimental determination of acoustic properties using a two-microphone random-excitation technique”. *J. Acous. Soc. America*, **61**(5), pp. 1362–1370.
- [37] Vignat, G., 2020. “Dynamique de l’injection et de la combustion dans des flammes de spray swirlées et couplage azimutal dans les foyers annulaires”. PhD thesis, Université Paris-Saclay, prepared at CentraleSupélec, Gif-sur-Yvette, France.
- [38] Durox, D., Schuller, T., Noiray, N., and Candel, S., 2009. “Experimental analysis of nonlinear flame transfer functions for different flame geometries”. *Proc. Combust. Inst.*, **32**(1), pp. 1391–1398.
- [39] Schuller, T., Poinso, T., and Candel, S., 2020. “Dynamics and control of premixed combustion systems based on flame transfer and describing functions”. *J. Fluid Mech.*, **894**, p. 1.
- [40] Noiray, N., Durox, D., Schuller, T., and Candel, S., 2009. “A method for estimating the noise level of unstable combustion based on the flame describing function”. *Intl. J. Aeroacoustics*, **8**(1), pp. 157–176.
- [41] Schuller, T., Durox, D., and Candel, S., 2003. “Self-induced combustion oscillations of laminar premixed flames stabilized on annular burners”. *Combust. Flame*, **135**(4), pp. 525–537.
- [42] Fanaca, D., Alemela, P., Hirsch, C., and Sattelmayer, T., 2010. “Comparison of the flow field of a swirl stabilized premixed burner in an annular and a single burner combustion chamber”. *J. Eng. Gas Turb. Power*, **132**(7).
- [43] Lee, T., Park, J., Han, D., and Kim, K. T., 2019. “The dynamics of multiple interacting swirl-stabilized flames in a lean-premixed gas turbine combustor”. *Proc. Combust. Inst.*, **37**(4), jan, pp. 5137–5145.